Improving Tracking Robustness Through Interference Using Pilot Signals with a Deeply Coupled Estimator

Logan Bednarz, Samer Khanafseh, Boris Pervan, *Illinois Institute of Technology*

BIOGRAPHY

Logan Bednarz obtained his Bachelor's and Master's Degree in Mechanical Engineering from Illinois Institute of Technology (IIT), in 2022. He is currently a Ph.D. candidate in Mechanical and Aerospace Engineering at IIT, as well as a Navigation Engineer at TruNav. His current research focuses on the development of an SDR platform to fuse GNSS/INS for a comprehensive PVT and fault detection platform. His research interests also include novel methods for IMU data generation - as well as using pilot signals and multi constellation signal planning, to subvert jamming and spoofing scenarios.

Dr. Samer Khanafseh is currently a Research AssociateProfessor at the Mechanical and Aerospace Engineering Department at IIT. He received his M.S. and Ph.D. degrees in Aerospace Engineering from IIT, in 2003 and 2008, respectively. Dr. Khanafseh has been involved in several aviation applications such as Autonomous Airborne Refueling (AAR) of unmanned air vehicles, autonomous shipboard landing for NUCAS and JPALS programs and Ground Based Augmentation System (GBAS). He published 13 journal articles and more than 30 conference papers. His research interests are focused on high accuracy and high integrity navigation algorithms for close proximity applications, cycle ambiguity resolution, high integrity applications, fault monitoring and robust estimation techniques. He was the recipient of the 2011 Institute of Navigation Early Achievement Award for his outstanding contributions to the integrity of carrier phase navigation systems.

Dr. Boris Pervan is a Professor of Mechanical and Aerospace Engineering at IIT, where he conducts research on advanced navigation systems. Prior to joining the faculty at IIT, he was a spacecraft mission analyst at Hughes Aircraft Company (now Boeing) and a postdoctoral research associate at Stanford University. Prof. Pervan received his B.S. from the University of Notre Dame, M.S. from the California Institute of Technology, and Ph.D. from Stanford University. He was the recipient of the IIT Sigma Xi Excellence in University Research Award, Ralph Barnett Mechanical and Aerospace Dept. Outstanding Teaching Award, Mechanical and Aerospace Dept. Excellence in Research Award, IIT University Excellence in Teaching Award, IEEE Aerospace and Electronic Systems Society M. Barry Carlton Award, RTCA William E. Jackson Award, Guggenheim Fellowship (Caltech), the Albert J. Zahm Prize in Aeronautics (Notre Dame), and the Institution of Navigation Kepler Award. He is an Associate Fellow of the AIAA, a Fellow of the Institute of Navigation (ION), and Editor-in-Chief of the ION Journal Navigation.

ABSTRACT

This paper shows the viability of improving tracking robustness of global navigation satellite systems (GNSS) pilot signals in high interference and/or jamming conditions by deep coupling with inertial sensors using a Kalman filter. In this work, we confront the limiting factors of typical tracking loops, including the dependency on pre-filtering or coherent averaging (Julien 2014), the adverse correlation effects that would otherwise come from integrating over the Doppler frequency of the incoming signals (Borio et al. 2014, Julien 2014), biased inertial measurement sensor (IMU) accelerometer/gyroscope noise inputs, and local oscillator (LO) phase noise (Misra and Enge 2001). Our deeply coupled Kalman filter is designed to specifically confront these limitations. The use of a deeply coupled Kalman filter also allows for a well-defined analysis of the integrity of the filter's best state estimate, which can be used to expose noise sources which most quickly degrade estimate quality. Using this analysis, the robustness of this and similar estimators to all noise levels given all available hardware can be extended and defined, and thus provide a valuable asset not only to robustness, but also to estimator and sensing scheme design. We show that this early version of our tracking algorithm is able to maintain signal lock in carrier to noise density ratios as low as 4 dBHz.

I. INTRODUCTION

Global Navigation Satellite Systems (GNSS) signals are invaluable for many day-to-day navigation applications, but they also must be dependable in high-interference environments. Given that GNSS signals are so critical for a variety of applications and have such widespread use, they can become targets for malicious jamming attacks. To compound this issue, commercial jammers costing as little as 40 USD are available for purchase online (Mukherji and Chandele 2022).

Over the years, several anti-jamming methods have emerged to combat these threats. For instance, combined data-pilot signal acquisition (Borio et al. 2014), dual-antenna receiver implementations (Broumandan et al. 2020), and polarization-sensitive arrays (Sun et al. 2022) represent a subset of the strategies employed to enhance signal reconstruction quality at the GNSS receiver. It's well-understood that longer integration times correlate positively with the carrier to noise density ratio (C/N0), which serves as a metric of signal reconstruction quality (Borio et al. 2014, Julien 2014). This understanding naturally leads to a seemingly straightforward mitigation approach: extending the coherent integration time of the tracking loops. However, this is where challenges arise. Conventional Phase Lock Loop (PLL) and Delay Lock Loop (DLL) tracking schemes using data-carrying signals often struggle to extend integration times due to ambiguities in the navigation data bits. Additionally, these schemes might not effectively account for system dynamics during integration, typically operating under the assumption that signal parameters remain constant during said integration.

Our approach builds upon the foundational work presented in (Zhao et al. 2019). At its core, our method relies on a deeply coupled Kalman Filter, which has been tailored to accommodate fluctuations in Doppler frequency and code delays. This filter fuses IMU and GNSS measurements to generate precise user state estimates. Our approach takes a theoretical deviation from (Zhao et al. 2019) in its handling of ambiguities in the navigation data bit. Instead of utilizing their adaptive model, we leverage the pilot signal to eradicate the ambiguities introduced by the navigation data bit.

The term “coherent averaging” in this context deserves special attention. While our method doesn't literally extend the coherent integration of our pilot signal measurements, the Kalman Filter plays a crucial role in mimicking this effect. Specifically, the filter's low-pass action reduces the state covariance until it reaches a steady state value. For our purposes, we interpret this stabilization as marking the conclusion of the coherent averaging period.

This work will demonstrate that the PLL and DLL can be replaced by the proposed deeply coupled Kalman filter to capture the effect of extending the coherent integration time of our measurements while constantly accounting for the changing dynamics of the system. We develop this filter to coast through jamming and high interference events - implying that we do not “cold start” during a jamming event, for instance.

II. KALMAN FILTER MODEL

In this section, we develop the components required for the operation of our proposed Kalman filter. The Kalman filter, in general, requires both a measurement model and a set of dynamics that can account for the independent states this measurement model contains.

A typical signal measurement at the GNSS receiver is presented below:

$$y = aR(t - \Delta\tau)\exp\{i(2\pi\Delta\theta)\} + n \qquad (1)$$

where we define a as the signal amplitude, $R(t - \Delta\tau)$ as the autocorrelation function evaluated at $\Delta\tau$, the deviation between the actual spreading code delay and the signal local replica’s argument of the spreading code delay, $\exp\{i(2\pi\Delta\theta)\}$ represents the in-phase and quadrature-phase components of the incoming signal, which has a complex argument defined by the deviation between the incoming signal’s phase and the local replica’s account of that phase, and n represents additive white gaussian noise (AWGN). It's crucial to note that this initial form of measurement assumes the integration of the incoming signal and local replica over one spreading code period. The rationale behind this representation, though intricate, will be elucidated later.

Let’s now adopt an alternative representation of τ and θ for use in the coming dynamic modeling:

$$\theta_{total} = \frac{1}{\lambda}(\varrho - I + T + c(\delta t_r - \delta t_s) + \lambda N) \qquad (2)$$

$$\rho\frac{1}{c} = \tau = \frac{1}{c}(\varrho + I + T + c(\delta t_r - \delta t_s)) \quad (3)$$

where θ_{total} represents the total phase from the space vehicle's transmitter to our receiver, λ represents this signals wavelength, ϱ represents the true range between the receiver and transmitter, I and T represent the ionospheric and tropospheric delays, respectively, c represents the speed of light δt_r and δt_s represent the receiver and space vehicle time offsets, respectively, and finally N represents the integer cycle ambiguity.

Considering the above representation, let's inspect the implications of substituting θ_{total} from equation (2) in equation (1):

$$y_I = aR(t - \Delta\tau)\cos(2\pi\Delta(\frac{1}{\lambda}(\varrho - I + T + c(\delta t_r - \delta t_s) + \lambda N))) + n \quad (4)$$

where we have extracted only the in-phase component of (1) for simplicity, although the same procedure can be applied to the quadrature term. Here we see that the argument of the cosine is shifted by a factor of $2\pi N$, which is an integer multiple of 2π radians. Thus, θ_{total} and θ can be used interchangeably in (1).

Before we continue, note that the use of ϱ as a state will result in a direct positioning algorithm and that the integer ambiguity does not need to be resolved to estimate this position. We have now substantiated that substituting (2) and (3) into (1) captures a new representation of the signal, which we will have to establish dynamics for.

Since the goal is to coast through an interference event, we assume that we have access to the ephemeris (navigation message), and therefore can compute the satellite position and have a correction for δt_s. This results in the following unique states to be modeled by dynamics:

$$x_{in} = \begin{pmatrix} a & \varrho & I & T & \delta t_r \end{pmatrix}^T \quad (5)$$

The example dynamic models implemented here are a specialized 1D inertial measurement unit (IMU) model and a clock phase error model. We will show that these two models capture the states in (5). We begin with the range which we can express as:

$$\varrho = r_{sv} - r_r \quad (6)$$

where r_r represents the receiver position and r_{sv} represents the space vehicle's position. Note that this relation is algebraic, so we can substitute (6) into our measurement model.

Next, we employ the linearized IMU equations of motion to model the receiver position.

$$\delta\dot{r}_r = \delta v \quad (7)$$

$$\delta\dot{v} = f^u + b - 2\Omega_{i/e}\delta v + g + w_{acc} \quad (8)$$

$$\dot{b} = -\frac{1}{\tau_b}b + w_b \quad (9)$$

where v represents the receiver velocity, f^u represents the unbiased accelerometer input, b represents the accelerometer bias, $\Omega_{i/e}$ represents the rate of rotation of the earth, g represents the gravitational acceleration on earth, τ_b represents the time constant of the first order Gauss Markov process (FOGMP) for the bias state. δ indicates a deviation of a state linearized about some given point. The process noise on these equations comes from the AWGN sources w_{acc} and w_b for their respective processes. Finishing the set of dynamics, we use a FOGMP similar to (9) for the ionospheric and tropospheric delays, and a two-state clock model for the clock time bias.

We see that our new set of states produces the state vector we will use for our analysis:

$$x = \left(a \;\; r_r \;\; v \;\; I \;\; T \;\; \delta t_r \;\; \dot{\delta t_r} \;\; b\right)^T \tag{10}$$

III. ASSERTIONS, LIMITATIONS

Chronologically, let's evaluate what each equation reveals about the system we're analyzing. Equations (2) and (3) are presented in an algebraic form, indicating certain limitations. Specifically, factors such as multipath effects, phase windup, and ionospheric scintillations are not accounted for in the preliminary analysis. Equations (8) and (9) represent a stark simplification when contrasted with the conventional IMU equations of motion. The attitude and rotation matrices are absent, because of the 1-D assumption made earlier. With this understanding, when we scrutinize Equation (6), it suggests that both r_r and r_{sv} must be represented in a coordinate system that aligns with the line of sight (LOS). Consequently, any motion in the receiver's position should strictly occur along this LOS. With this in mind, we are primed to understand this paper as an initial study of the feasibility of such a method in its simplest possible form. Even with this model, we have the reach to understand the benefits of employing this filter, rather than a PLL/DLL scheme.

IV. LINEARIZATION

Since we employ a Kalman filter, which is the optimal *linear* estimator, we cannot utilize our measurement in its current form. Instead, we will use a Taylor series expansion for each state and linearize about the Kalman filter's time update in our measurement integration period; this means we realize the Kalman filter as an extended Kalman filter (EKF).

We should understand that the sine and cosine components of the measurement have defined derivatives everywhere, but $R(t - \Delta\tau)$ does not. In fact, this is why we accumulate the incoming measurements at all. We *could* represent the measurement as the instantaneous multiplication of the local replica and incoming signal, but the spreading code is laden with undefined derivatives and highly nonlinear. By accumulating over one code period, we need only to contend with the derivatives of this autocorrelation function.

We employ an early and late correlator for both the in-phase and quadrature-phase component of the accumulated signal. We use these as measurements meant to bound the real code phase. This is shown in a figure below:

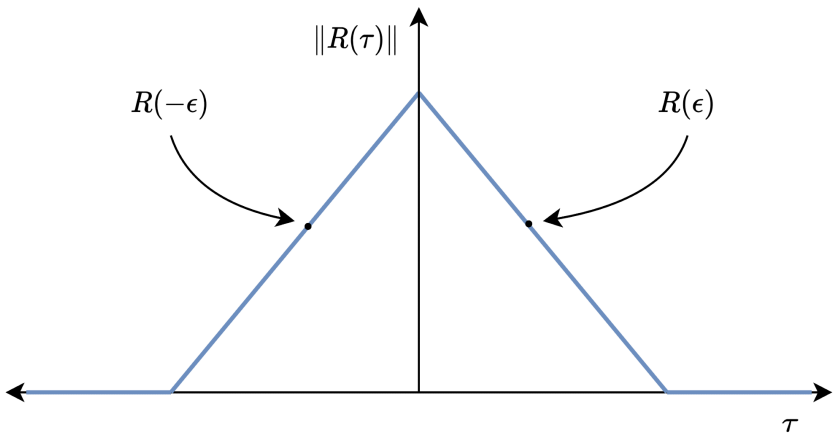

Figure 1: *Example ACF with a representation of the early and late correlators example values. Note that the early and late correlators are meant to capture the value of the ACF around the maximum value, thus providing a means to bound the peak, as well as evaluate the derivative of the ACF, when linearizing, only where it is defined. Epsilon represents the correlator's shift from the expected code phase.*

With all these pieces in place, we summarize the filter operation, pictorially, below:

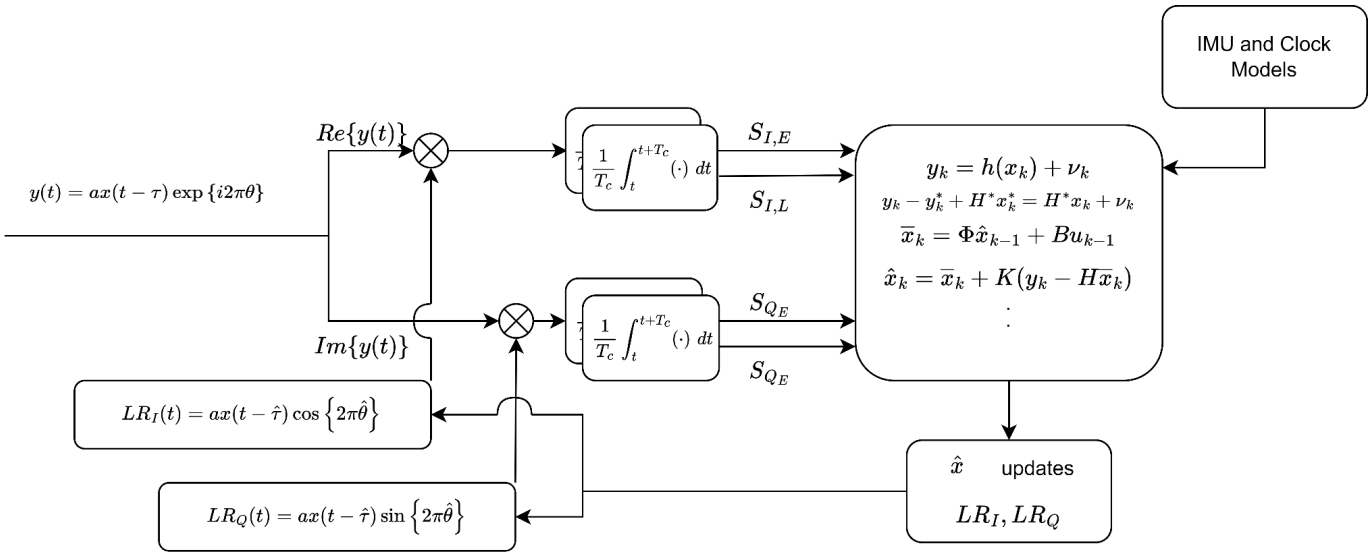

Figure 2: *Frequency response between input accelerometer noise and output position. The time constant here was taken to be 33 seconds.*

Note that the top branch of the diagram involves extracting only the real part of the signal, and the imaginary part enters into the lower branch. Not pictured are the low pass filtering operations after the correlation step.

Here H represents the linearized observation matrix, h is the nonlinear observation function, Φ represents the state transition matrix, $\bar{x}$ and $\hat{x}$ represent the time updated and measurement updated state vectors, B represents the matrix of coefficients for u - the control input, K is the Kalman gain, ν is the measurement noise, $S_{I,E}$ and $S_{I,L}$ represent the integrated in-phase and $S_{Q,E}$ and $S_{Q,L}$ represent the integrated quadrature-phase measurements, respectively.

V. THEORETICAL ANALYSIS

Next, we conducted a feasibility analysis with the aim to determine the following:

- Identify which factors limit our effective coherent integration time
- Describe the performance under a range of $\frac{C}{N_0}$
- Determine time constants, and effective filtering bandwidth of EKF
- Compare time constants to coherent integration period of PLL/DLL scheme

Starting with the limiting factors of our effective coherent averaging time, we examine the transfer functions of our models between our process noise inputs and our state outputs. These obtained using the Laplace Transform:

$$L\{\dot{x}\} = L\{Ax + Bu + Gw\}$$
$$X(s) = [sI - A]^{-1}[BU(s) + GW(s)] \quad (11)$$

Examining each time constant, the shortest was found to be between the accelerometer noise and the position output. The frequency response is shown below:

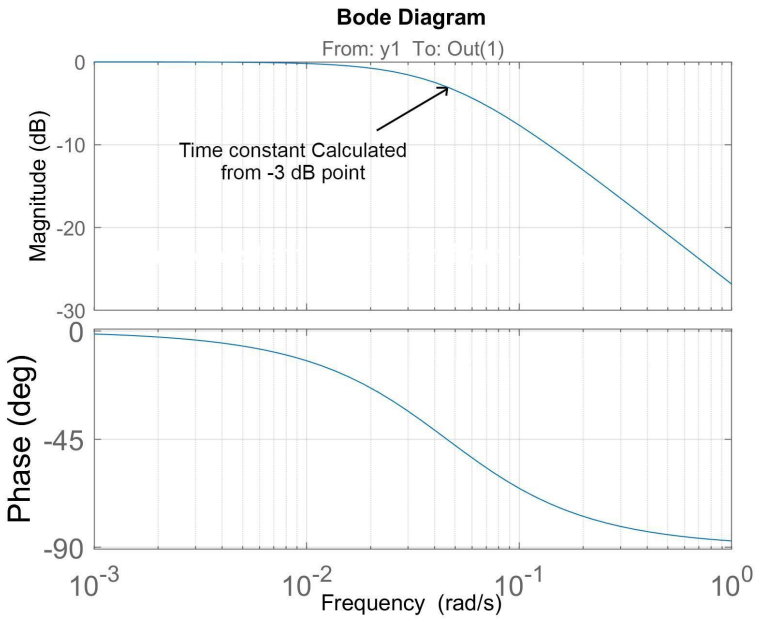

Figure 3: *Frequency response between input accelerometer noise and output position. The time constant here was taken to be 33 seconds.*

Based on the filter's frequency response, we determined its time constant to be approximately 33 seconds. This can be conceptually understood as the duration over which averaging persists. Notably, this suggests an equivalent coherent averaging time that vastly exceeds the conventional limit of 20 milliseconds for data-carrying signals. This result was obtained for a $\frac{C}{N_0}$ of 10 dB-Hz and the following IMU specifications were used:

	Accelerometers
Bias Stability	$\pm$ 5 mg
Random walk	57 $\mu g/\sqrt{Hz}$
Bias in-run instability	14 μg
Bias time constant	3600 s

These are the same specifications used in (Kujur et al. 2023). Note that the gyroscope information is not included in our analysis since we take the hypothetical 1D analysis described in the dynamic models.

We utilize the algebraic Riccati equation to analyze the steady state position standard deviation under for different values of $\frac{C}{N_0}$.

The results of this analysis are shown below:

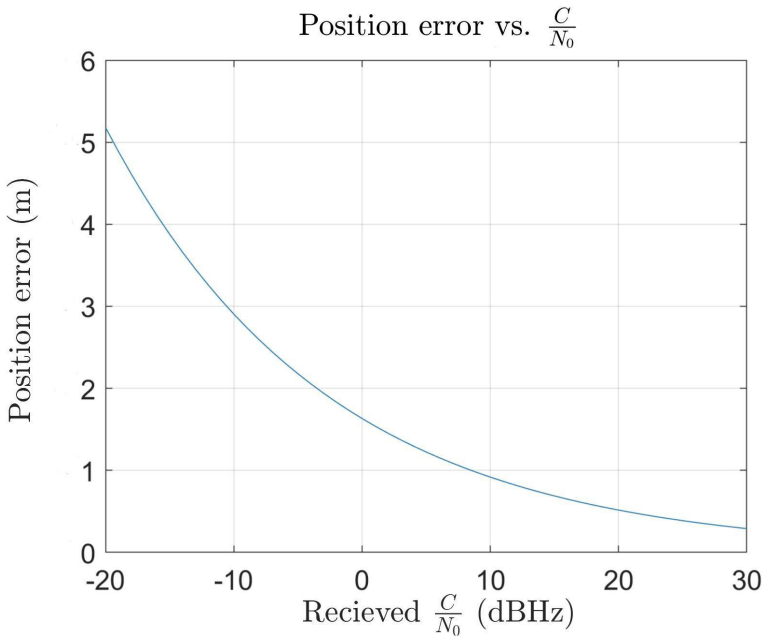

Figure 4. *Position standard deviation plotted against the received signal's* $\frac{C}{N_0}$. *Note that the linearization of the model degrades as state error increases, which can impart effects on the covariance that are not captured here.*

Examining this figure reveals a promising performance at extremely low carrier to noise densities, but these are produced under a simplified 1-D model and, in some of the cases shown above, assuming that linearization still holds for position errors on the order of 10s of meters (considering the standard deviation results).

For these and all following analyses, $\frac{C}{N_0}$ was calculated using the wide-band versus narrow-band method:

$$\frac{C}{N_0} = 10\log_{10}\left(\frac{(I_p^{\,2}+Q_p^{\,2})}{(I_E^{\,2}+Q_E^{\,2})+(I_E^{\,2}+Q_E^{\,2})}\right) dBHz \qquad (12)$$

At this point, this pilot signal-based implementation promises sweeping improvements in the performance of tracking over comparable methods, which typically report successful tracking for signals with $\frac{C}{N_0}$ in the range of ~8-10 dB-Hz (Ziedan 2005, Ziedan 2006). Additionally, the time constant allows for averaging over about 1500 times as long as for data-carrying signals.

VI. SIMULATION AND TESTING

Here we describe the simulation scenario and present some preliminary results of the filter. As was established in the assertion and limitations section, the scenario is highly specialized for this initial testing of the filter. The receiver dynamics involve 1D movement along the line of sight between the receiver and satellite. Additionally, the receiver velocity was enforced to be constant. Besides the receiver dynamics, the two-state clock model used a bias process noise of $1 \cdot 10^{-8}$ seconds and a bias drift process noise of $5 \cdot 10^{-10}$ seconds/second.

Next, a Skydel GNSS simulator was used to generate radio frequency data that was using a USRP device. This is represented, pictorially, below:

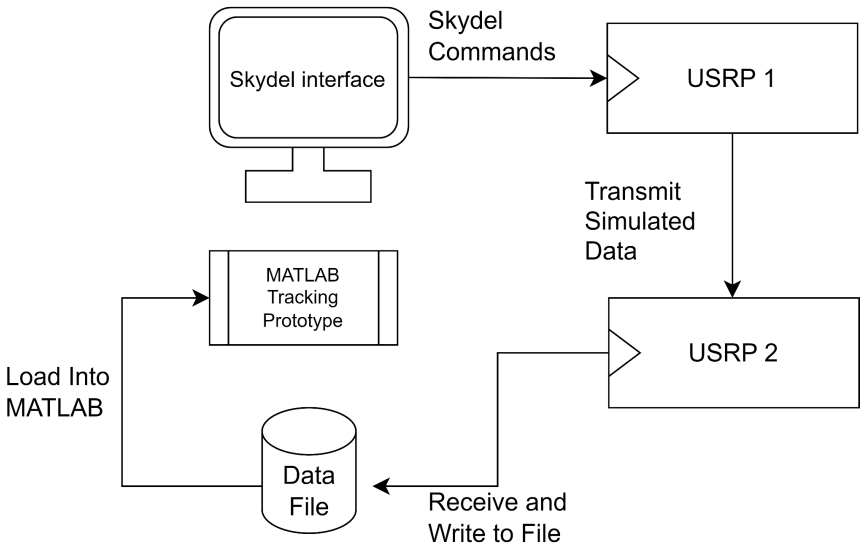

Figure 5: *Experimental setup.*

During the simulation, the $\frac{C}{N_0}$ was altered in time using MATLAB's "awgn" function, which allows for mixing the RF measurements with a noise profile. This mixing was used on the incoming RF data to simulate high interference. The measurement covariance, which is defined by the inverse of the $\frac{C}{N_0}$, converted from the logarithmic dB-Hz scale, to a linear scale.The performance of the tracking algorithm against the $\frac{C}{N_0}$ profile is shown below.

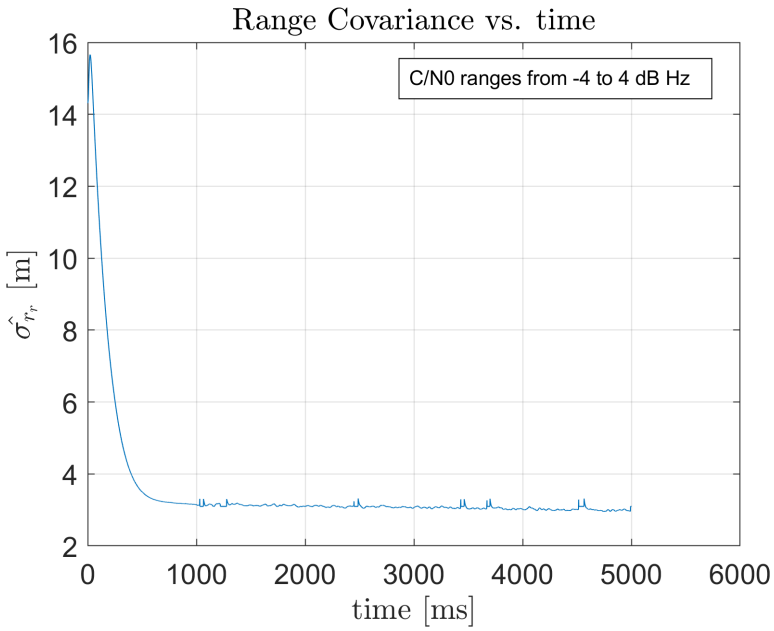

Figure 6: *Position standard deviation plotted time. Note that the steady state position standard deviation is about 2.5 meters.*

The steady state covariance shown matches well with the prediction in Figure 4 for a received $\frac{C}{N_0}$ of 0 dB-Hz; however, the $\frac{C}{N_0}$ profile indicated that the mean value was about 4 dB-Hz with a 7 ms period of $\frac{C}{N_0}$'s at -4 dB-Hz starting near one second. At 4 dB-Hz the expected steady state position standard deviation was about 1 meter.

The steady state value was reached in 5 seconds, rather than the predicted 33 seconds, but appealing back to our analogy about

the meaning of this time constant, this implies that the effective coherent integration time for the filter in this case is 5 seconds - vastly higher than the 20 ms typically seen in other tracking loops.

VII. FUTURE WORK

The results and methodologies presented in this paper provide a foundation for several directions of further investigation and development.

3D IMU Integration: While the current study was limited to a 1D IMU model with zero attitude, future work will generalize the mathematical development of the dynamic model to 3D. This will account for the full range of motion and dynamics in three-dimensional space, providing more comprehensive navigation solutions and improving the fidelity of the tracking method.

Multiple Space Vehicles (SV) Tracking: The current method will be extended to tracking signals from multiple space vehicles simultaneously—i.e., in a single state vector. This multi-SV approach may provide enhanced position accuracy and redundancy, especially in challenging environments or scenarios with partial satellite visibility. The system's architecture may evolve to resemble a vector tracking approach, as detailed in (Jin 2012).

Extended Kalman Filter (EKF) Sensitivity Analysis: Given the inherent non-linearities and complexities in the GNSS signal model used, the sensitivity of the Extended Kalman Filter (EKF) to higher state deviations will be closely examined. For instance, it was noted that for high phase error, the model linearization may become poor, leading to a low-fidelity model.

By embarking on these future research directions, the aim is to make GNSS signal tracking more resilient to jamming and interference.

VIII. CONCLUSION

Presented here is a novel method for signal tracking that involves leveraging the dataless nature of the pilot signal to achieve a dramatically increased effective coherent integration time. Though the system is simplified for this early analysis, future work generalizing this method to 3D scenarios and multiple space vehicles shows promise for this as a direct positioning and vector tracking-type filter that may be able to perform in high interference and jamming conditions.

Importantly, the modularity of our model stands out. It allows a thorough examination of the filter's behavior across various noise environments, incorporating an extensive range of oscillators and IMU configurations. This versatility ensures users can empirically gauge the influence of different hardware configurations—whether in their possession or prospective acquisitions—on performance metrics tailored to their specific applications.

Even in its nascent form, our tracking algorithm has demonstrated an ability to maintain signal lock in scenarios with carrier to noise density ratios as low as 4 dBHz. As we look ahead, we remain optimistic about the broader implications of this work, not only in fortifying GNSS robustness to high interference and jamming conditions.

REFERENCES

D. Borio, C. O'Driscoll, and G. Lachapelle, "Composite GNSS Signal Acquisition over Multiple Code Periods," IEEE Transactions on Aerospace and Electronic Systems, vol. 46, no. 1, pp. 193-206, Jan. 2010.

A. Broumandan, T. Taylor, D. Anklovitch, and S. Kennedy, "Robust Dual-Antenna Receiver: Jamming/Spoofing Detection and Mitigation," Proceedings of the 33rd International Technical Meeting of the Satellite Division of The Institute of Navigation (ION GNSS+ 2020), Sep. 2020, pp. 1515-1532.

S. Jin, Ed., Global Navigation Satellite Systems: Signal, Theory and Applications. InTech, 2012. doi: 10.5772/1134

Julien, O.r, ”Carrier-Phase Tracking of Future Data/Pilot Signals,” Proceedings of the 18th International Technical Meeting of the Satellite Division of The Institute of Navigation (ION GNSS 2005), Long Beach, CA, September 2005, pp. 113-124.

B. Kujur, S. Khanafseh, and B. Pervan, "Experimental Validation of Optimal INS Monitor against GNSS Spoofer Tracking Error Detection," Proceedings of IEEE/ION Position, Location, and Navigation Symposium (PLANS), Monterey, CA, Apr. 2023.

V. Mukherji and A. K. S. Chandele, "GNSS Jamming: An Omnipresent Threat," Geospatial World, 2022. [Online].

P. Misra and P. Enge, Global Positioning System: Signals, Measurements, and Performance, 2nd ed. Ganga-Jamuna Press, 2001, ch. Precise Point Positioning with Carrier Phase.

Y. Sun, J. Xie, C. Han, L. Wang, and M. Tao, "An RF Front-End Optimal Selection Scheme for Reconfigurable Anti-Jamming Polarization-Sensitive Array with Application to GNSS," Proceedings of the 35th International Technical Meeting of the Satellite Division of The Institute of Navigation (ION GNSS+ 2022), Denver, CO, Sep. 2022, pp. 2153-2162.

Zhao, W., Pervan, B., ”IMM Methods for Carrier Phase Tracking and Navigation Data Bit Estimation Through Interference”, Proceedings of the 2019 International Technical Meeting of the Institute of Navigation, Reston, VA. Jan. 2019.

Ziedan, N. I., "Extended Kalman Filter Tracking and Navigation Message Decoding of Weak GPS L2C and L5 Signals," Proceedings of the 18th International Technical Meeting of the Satellite Division of The Institute of Navigation (ION GNSS 2005), Long Beach, CA, September 2005, pp. 178-189.

Ziedan, N. I., "Extended Kalman Filter-Based Deeply Integrated GNSS/Low-Cost INS for Reliable Navigation Under GNSS Weak Interrupted Signal Conditions," Proceedings of the 19th International Technical Meeting of the Satellite Division of The Institute of Navigation (ION GNSS 2006), Fort Worth, TX, September 2006, pp. 2889-2900.